ELSEVIER

Chemical Physics 228 (1998) 185–203

Chemical Physics

The role of the initial population of molecular vibrations in surface photochemistry

S. Thiel, T. Klüner *, M. Wilde, K. Al-Shamery, H.-J. Freund

Fritz-Haber-Institut der Max-Planck-Gesellschaft, Faradayweg 4–6, D-14195 Berlin, Germany

Received 25 August 1997; accepted 17 October 1997

Abstract

In a one-dimensional wavepacket study the role of thermal population of molecular vibrations within surface photochemistry is studied using a model potential adopted to the system $NO/Cr_2O_3(0001)$. Simulations are made concerning the temperature dependence of the efficiency for UV-laser induced desorption and of velocity distributions. The course of these observables as a function of temperature is strongly dependent on the lifetime of the excited state. The results are compared with experimental results on the temperature dependence of the non-thermal desorption of NO from the $Cr_2O_3(0001)$ surface after excitation at 6.4 eV. The experimentally observed increase of desorption cross-sections by about a factor of 2 when changing the surface temperature between 100 and 300 K is simulated when assuming an average resonance lifetime on the order of 10 fs. The experimentally found increase of translational energy with increasing surface temperature by ~ 100 m/s is also consistent with theoretical results. © 1998 Elsevier Science B.V.

Keywords: Surface photochemistry; Wavepacket dynamics; Desorption cross-section; Velocity distributions

1. Introduction

In the early days of laser-induced surface photochemistry one was interested in populating individual adsorbate vibrations using infrared lasers to induce surface reactions [1]. The idea based on a concept proposed by Lethokov was to prepare a favourable precursor state for the reaction, via local excitation of the bond to be broken with the aim to control the route of elementary chemical reactions [2]. One application was suggested to be isotope separation. At this time only nanosecond lasers with a limited wavelength tunability were available. Normally, more than one laser photon was needed to excite the system above the dissociation threshold. It turned out that mainly surface heating was observed as the energy redistribution processes (IVR = intramolecular vibrational redistribution) leading to phonon excitation were fast on the time scale of the laser pulses used. However, in the field of gas-phase photochemistry vibrationally mediated photochemistry in small molecules has been demonstrated [3]. The mild laser-induced thermal desorption using infrared laser light found its application in analytical chemistry such as laser mass spectroscopy [4]. The surface molecular dynamicists, on the other hand, turned to electronically induced surface processes. DIET (desorption induced by electronic transition) was one of the major research activities. Particularly measurements on final quantum state distributions of

* Corresponding author.

PII S0301-0104(97)00326-1

the desorbing molecules turned out to give a major impact into the understanding of the elementary processes [5–7]. Recently attempts were made again to take up the idea of vibrationally mediated photochemistry at surfaces for example via a combined vibrationally IR–UV DIET scheme [8–10]. The reason for this is that enormous progress has been made with respect to laser technologies. Ultrafast lasers enabled experimentalists to study the coupling between electron–hole pairs and phonons to adsorbate vibrations in real time [11–13]. From these experiments it has been established that the processes take place on a picosecond time scale. Particularly findings using ultrashort laser pulses in the femtosecond regime gave new impulses as well. In those experiments it was found that multiple excitations within a single laser pulse resulted in a drastic non-linear increase of the desorption efficiency [14]. Branching ratios within chemical reactions can be altered by choosing the pulse intensity and duration as has been demonstrated for the CO oxidation on Pt(111) [15,16]. This effect was related to a pumping up within vibrational excitation of the relevant bond due to multiple excitations which increases the dissociation probability within this coordinate in further excitation cycles. We were therefore interested which impact different vibrational populations, i.e. populations of single vibrations as well as Boltzmann-distributed vibrational excitations have on a simple photoreaction such as a DIET process of a diatomic molecule and how this is influenced by the lifetime of the electronically excited state. We performed wavepacket calculations in a model potential adopted to the system $NO/Cr_2O_3(0001)$. For this system we can compare our theoretical calculations to an experiment in which the temperature dependence of the efficiency of the UV-laser induced desorption has been studied in addition to the temperature dependence of the final translational distribution of an individual rovibronic state. The experimental data will be presented in this paper together with our theoretical investigations.

2. Experimental setup

The experiments were carried out in a UHV chamber routinely used in our laser desorption experiments which has been discussed in detail elsewhere [17]. The chromium oxide was grown as epitaxial film on a clean Cr(110) single crystal surface in an atmosphere of 10^{-6} Torr of oxygen at 500 K followed by annealing the oxide to 1000 K. NO was desorbed normal to the surface with a pump laser pulse, a broad band excimer laser (Lambda Physik EMG 200, 15 ns, 1 mJ/cm^2) run at 6.4 eV. The desorbing molecules were detected in the gas phase parallel to the surface using (1 + 1) REMPI (resonance enhanced multi-photon ionisation) [19] and a tunable excimer (XeCl, Lambda Physik LPX 205 i cc) pumped dye laser (Lambda Physik LPD 3002). Time-of-flight spectra were obtained for individual rovibronic states by fixing the probe laser to the maximum of an individual transition and changing the time between desorption and detection. From the known distance and flight time the velocity of the detected molecules could be calculated. The ions produced via REMPI were detected perpendicular to the desorption and detection laser beam direction via a detector consisting of a repeller, a flight tube, microchannel plates and a phosphor screen.

The NO molecules were redosed onto the crystal kept between 90 and 300 K (depending on the experiment) after each laser desorption pulse using a pulsed molecular beam apparatus described elsewhere [18]. The base pressure within the measurement compartment did not exceed 3×10^{-10} Torr when the molecular beam was running.

3. Experimental findings

NO adsorbs as a chemisorbed species with a binding energy of ~ 1.0 eV (desorption temperature of 340 ± 20 K in thermal desorption spectra) at liquid nitrogen temperatures until a saturation coverage is reached. Further adsorption of a physisorbed species is then observed with strong indication of a related dimer formation [20]. Using a pulsed molecular beam allows us to exactly control the surface concentration by redosing a fixed amount after each laser shot so that an equilibrium concentration is sustained. The data presented here are desorption data from the chemisorbed species. This species is known to adsorb on top of the chromium ions with

an approximate tilt angle of 20–40° with respect to the normal of the surface [21].

3.1. Desorption cross-sections

The desorption cross-sections of NO desorbing from $Cr_2O_3(0001)$ were measured starting with a saturation coverage of the chemisorbed species of NO. For this purpose the substrate was predosed for 5 min with the pulsed molecular beam doser (4 Hz, pulse width 701 μs, pressure behind nozzle = 2 bar). After switching off the molecular beam the depletion of the adsorbate on the surface after exciting the system at 6.4 eV was followed by looking at the diminishing signal of the desorbing NO molecules in the gas phase as a function of photons impinged on the surface. The desorbing molecules were detected in a single rovibrational state at a fixed time delay between desorption and detection using REMPI. Assuming a first-order desorption kinetics the data can be analysed by plotting the logarithm of the intensity ($\ln(I/I_0)$) as a function of the number of photons impinged on the surface n_{ph}. We obtain a straight line for coverages down to $\frac{1}{5}$th of a saturation coverage of the chemisorbate with the slope being the desorption cross-section σ. For lower coverages a second line is observed corresponding to defect desorption. We shall here discuss only the cross-sections of the majority species (see also Ref. [20] for further details). We did not observe any dependence on the final rotational state of desorbing NO. The temperature dependence of the desorption cross-sections was obtained by keeping the crystal at a fixed temperature during the whole experiment and is shown in Fig. 1a. Though the error bars are relatively large one can clearly see that the desorption cross-sections increase with increasing temperature by about a factor of 2 in the temperature range of 90 to 260 K.

3.2. Velocity distributions

Time-of-flight spectra were obtained by measuring the desorption signal as a function of delay time between detection and desorption of a single rovibronic state. For each time delay the signal was averaged over 300 laser pulses. The coverage at the surface was kept constant by redosing the crystal after each laser desorption pulse via the molecular beam doser. Such a dosing allowed a background free detection of the desorbing molecules. From the known distance between detection laser and substrate the velocity distributions can be calculated. Fig. 1b shows as an example the velocity distribution of the $J'' = 7.5$, $v'' = 0$, $^2\Pi_{1/2}$ state for a desorption energy of 6.4 eV as a function of three different temperatures. The curves were normalized to the maximum of the distribution. A detailed discussion of the influence of the desorption energy and the rovibronic states of the desorbing molecules onto the shape of the velocity distributions including the possible influence of a precursor state is given in Ref. [20]. We want to focus in this paper onto the pure temperature dependence of the velocity distributions. The maximum of these is shifting towards higher velocities by ~ 200 m/s when comparing the data of 90 K to the data taken at 250 K. Fig. 1c shows a plot of the mean velocity obtained for a number of velocity distributions of the $J'' = 7.5$, $v'' = 0$, $^2\Pi_{1/2}$ state measured as a function of surface temperature. An increase in the mean velocities by ~ 100 m/s when changing the surface temperature from 90 to 300 K can be noticed.

4. Quantum mechanical simulations

In the following section of this paper a quantum mechanical explanation of the observed temperature dependence of the desorption cross-section and the velocity distribution is given. Saalfrank has shown in several wavepacket approaches with empirical potentials that vibrational excitation in the NO/Pt(111) and $NH(D)_3$/Cu(111) systems result in a drastic increase in the desorption probability [9,22–24]. Vibrational excitation was supposed to be generated mainly by infrared photons. In the approaches concerning the NO/Pt(111) system surface heating up to a temperature of 1000 K was also discussed as an alternative method to increase the desorption cross-section [23]. This influence of the temperature is again mentioned in density-matrix calculations on the NO/Pt(111) system, where a slight increase of the desorption yield by 5% is predicted if temperature is increased from $T = 0$ to 500 K [25]. In [26] the result of direct vibrational excitation by IR pho-

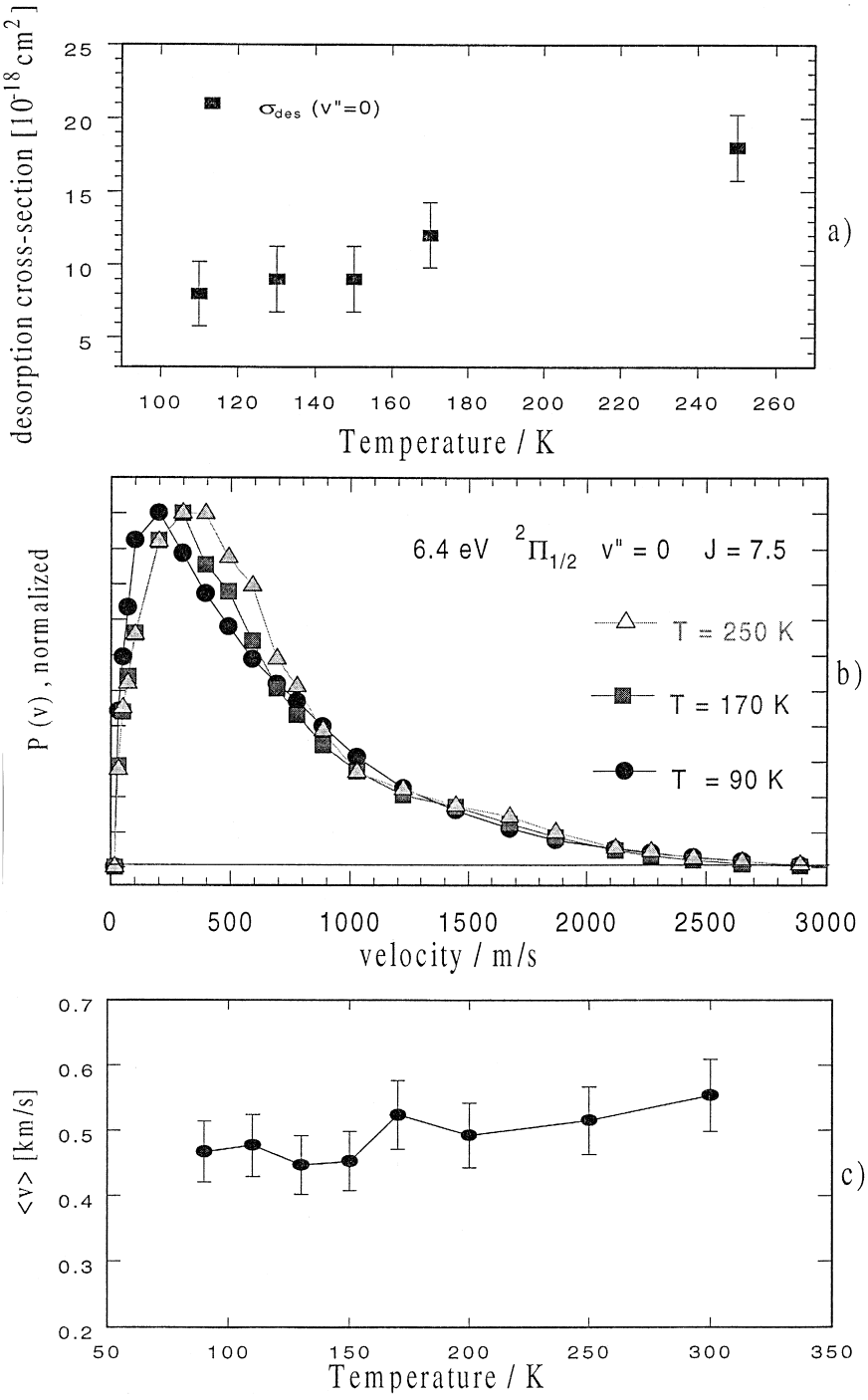

Fig. 1. Experimental LID results of NO from Cr_2O_3(0001) at 6.4 eV: (a) temperature dependence of the desorption cross-section σ; (b) velocity distributions for three different temperatures measured for $v'' = 0$, $J'' = 7.5$, the distributions are normalized to the peak maxima; and (c) temperature dependence of the mean velocities, deduced from the velocity distributions in (b).

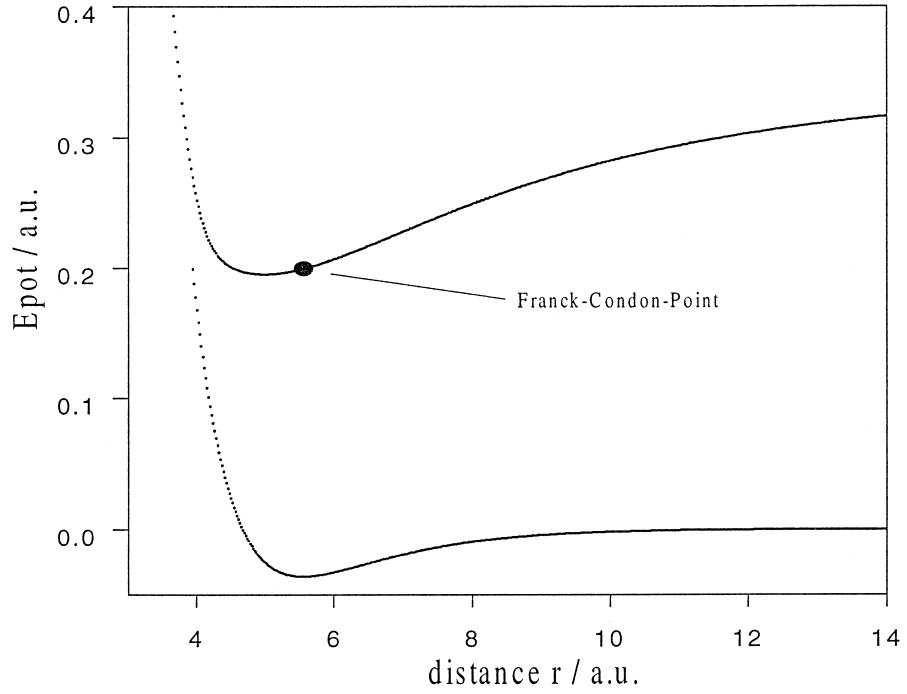

Fig. 2. One-dimensional potential configuration used in the quantum mechanical simulations throughout this work. The Franck–Condon point is shown as the starting point of all wavepackets that are propagated on the excited-state potential curve. The vertical shift between the two states matches the experimental excitation energy of 6.4 eV.

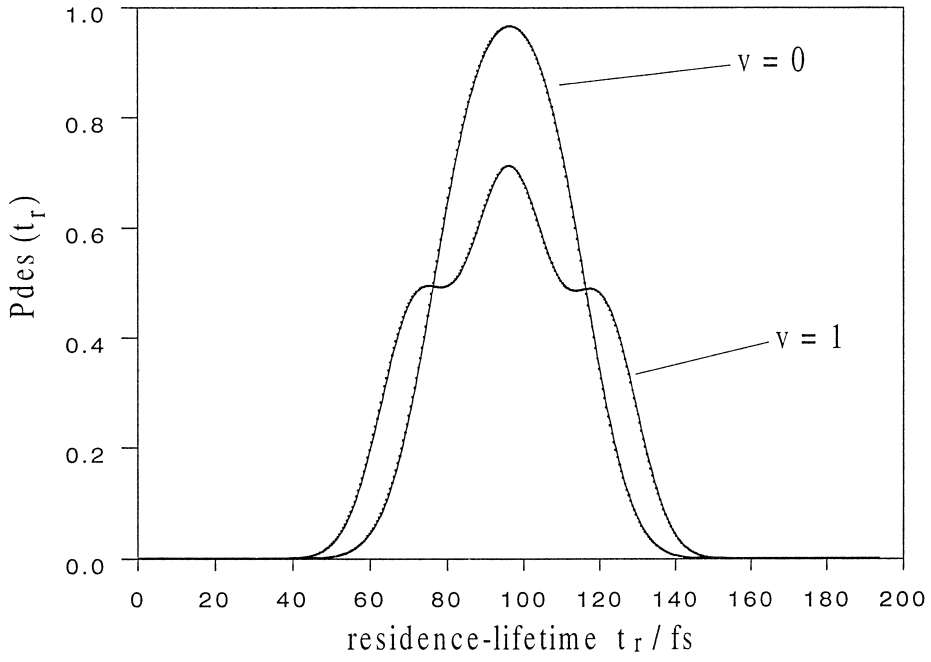

Fig. 3. Asymptotic desorption probability $P_{\mathrm{des}}(t_{\mathrm{r}})$ as function of fixed residence life-times t_{r} in the excited state. Shown are results for $\Psi_0(v)$ $(v = 0, 1)$ as initial wavefunctions.

tons is compared with the situation at $T = 1000\,\mathrm{K}$ for NO/Pt(111) using a density-matrix propagation technique by solving the Liouville–von Neumann equation.

Recently, Zhu et al. have investigated temperature effects in the photodesorption of methyl radicals from GaAs [8]. They explained the increase in the photodesorption yield in terms of an MGR picture

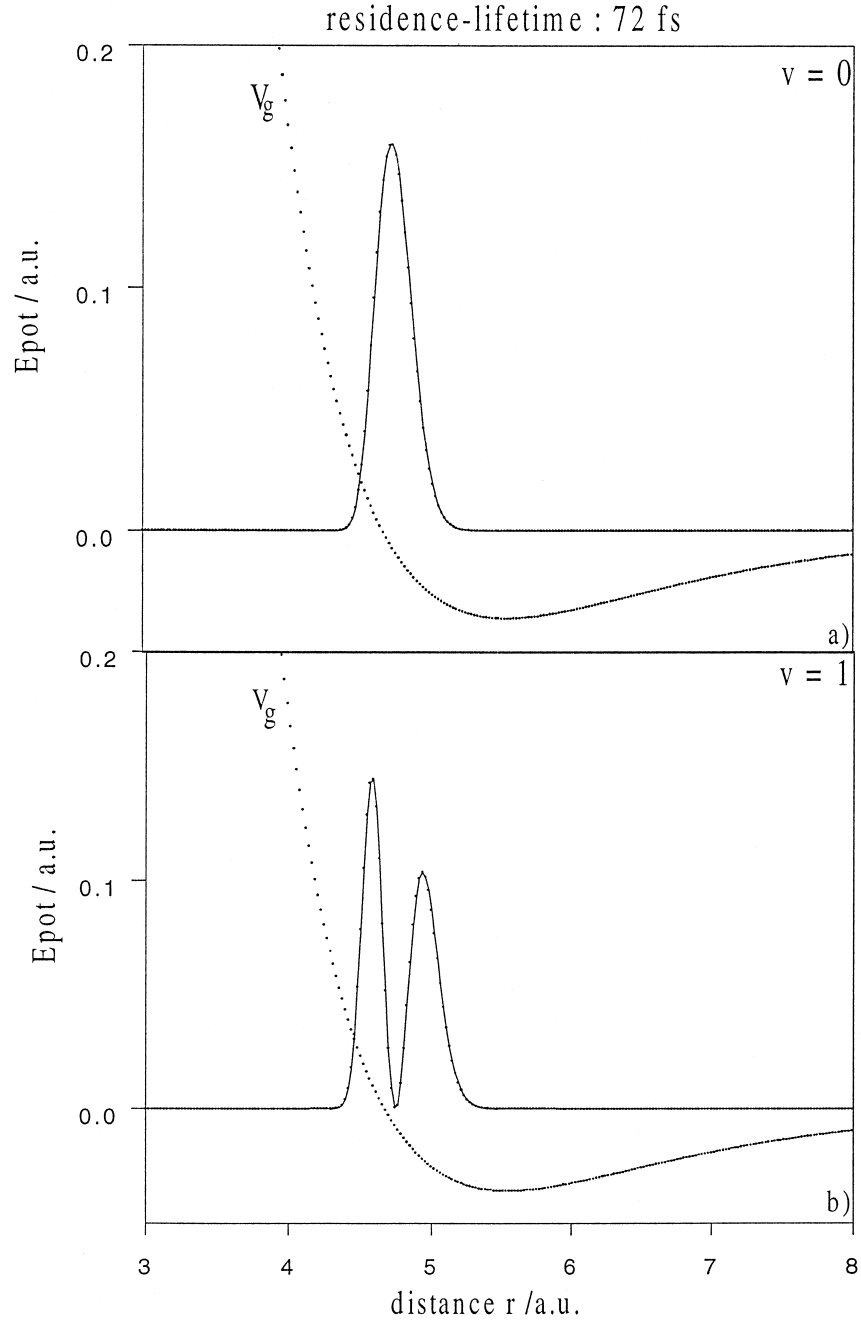

Fig. 4. Wavefunctions $\Psi_1(\nu = 0)$ (a) and $\Psi_1(\nu = 1)$ (b) at $t = t_r = 72$ fs after backtransfer onto the ground state V_g.

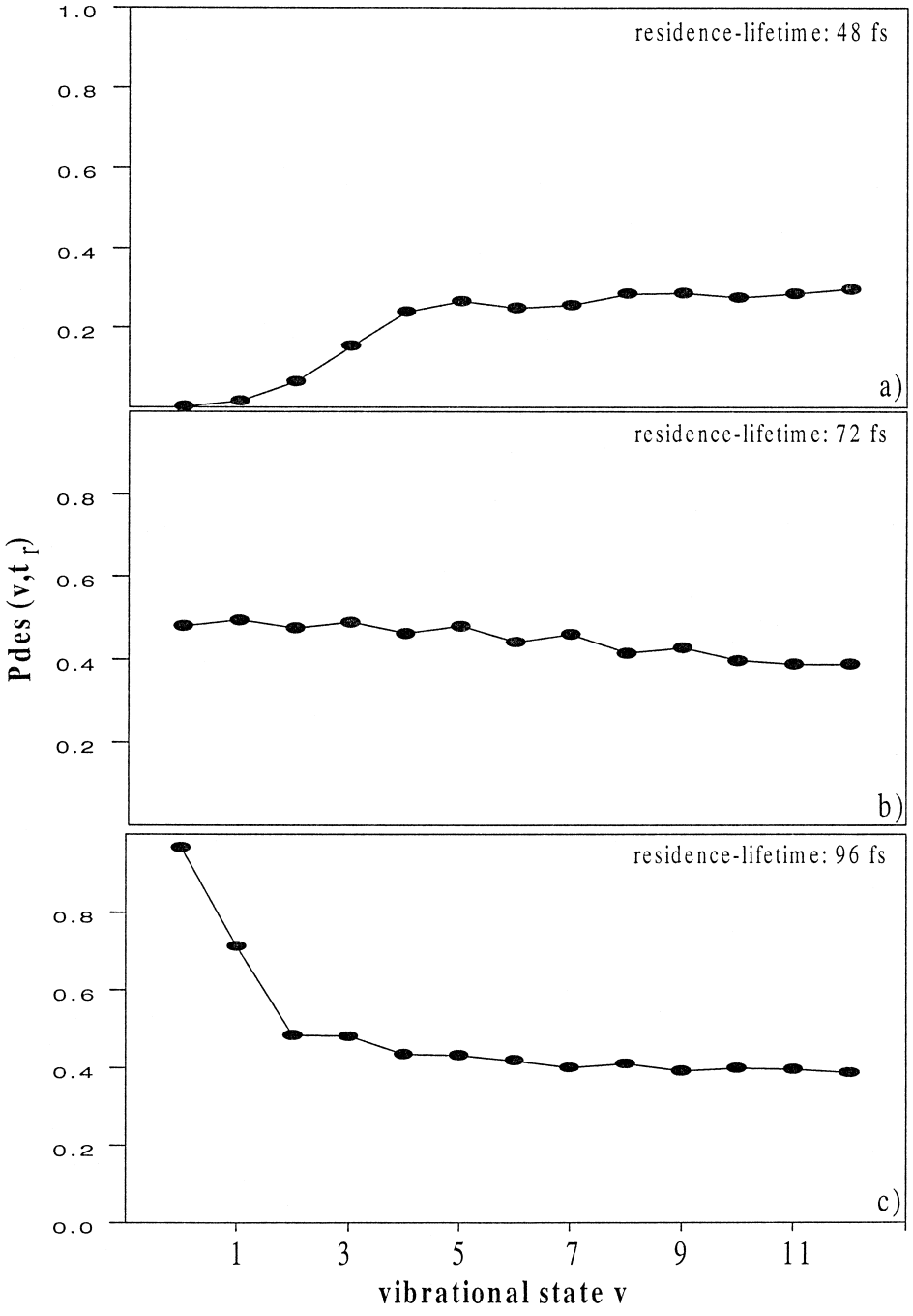

Fig. 5. Asymptotic desorption probability $P_{des}(v, t_r)$ for three fixed residence lifetimes as a function of the initial vibrational state v: (a) $t_r = 48$ fs; (b) $t_r = 72$ fs; and (c) $t_r = 96$ fs.

and discussed the role of vibrationally excited initial states. In that approach, parts of vibrationally excited wavefunctions cross a critical distance on the repulsive excited state earlier than the vibrational ground state because of their larger extension in coordinate space compared with the vibrational ground state.

In the context of our experimental results the temperature dependence of several observables in the DIET process of the system $NO/Cr_2O_3(0001)$ is studied systematically on the basis of two one-dimensional potential energy curves which are consistent with ab-initio calculations performed in our theory group [27]. A time-dependent wavepacket method will be applied, including the lifetime-averaging procedure proposed by Gadzuk and finally a Boltzmann weighting of the results. The next sections will deal with the computational methods and the potentials, followed by the presentation of some

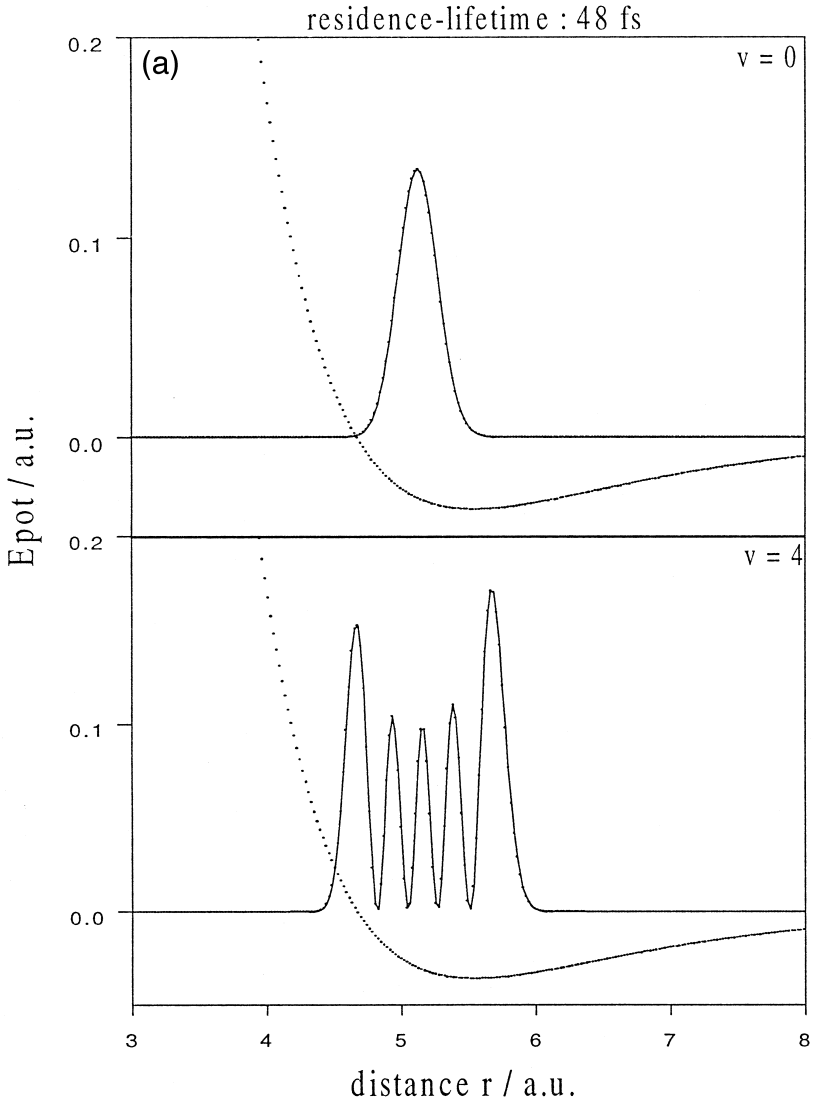

Fig. 6. Wavefunctions $\Psi_1(\nu = 0)$ and $\Psi_1(\nu = 4)$ at $t = t_r = 48$ fs (a) and at $t = t_r = 96$ fs (b) after backtransfer onto the ground state V_g. (a) and (b) are used to explain the increase and the decrease of $P_{des}(v)$ in Fig. 5a and c, respectively.

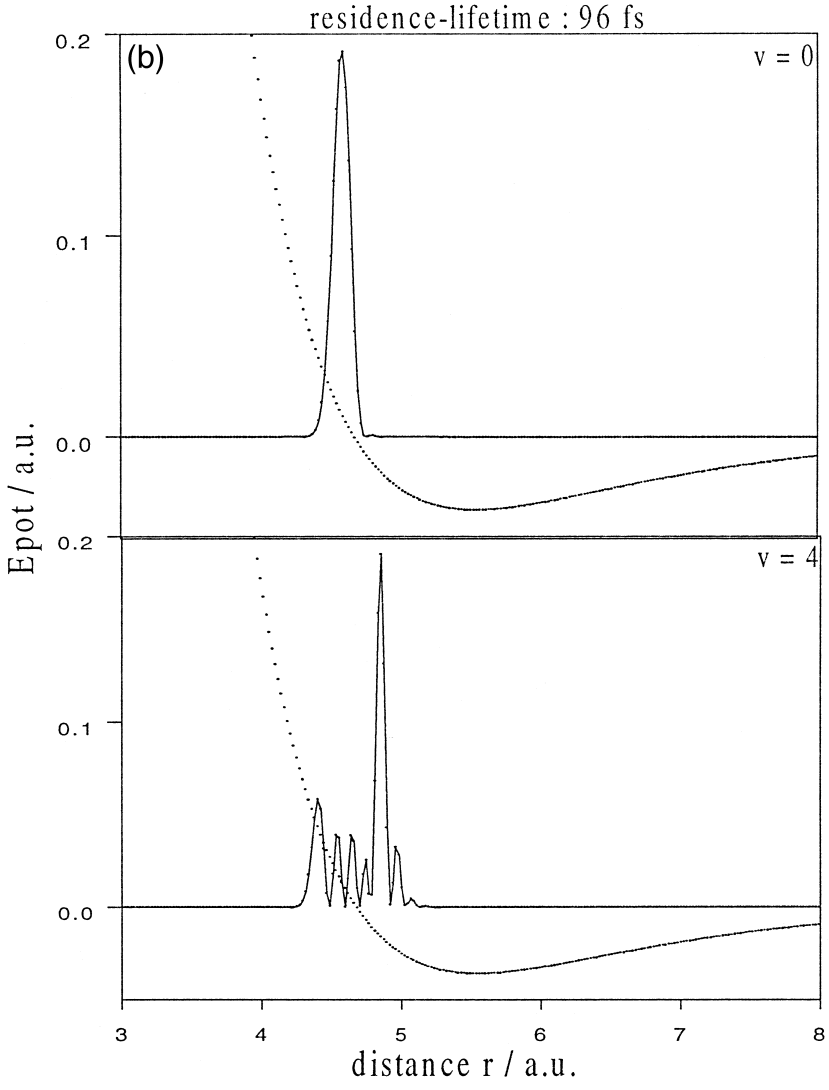

Fig. 6 (continued).

wavepacket dynamics with fixed lifetimes in the excited state. The quality of these simulations is then increased by applying a lifetime-averaging procedure to the former results. Finally, after including temperature as a parameter, the results are compared with experimental data.

4.1. Computational methods

In all wavepacket calculations presented in the following sections the time-dependent Schrödinger equation is solved by approximating the time-evolution operator $U(t)$ on a basis of complex Chebychev polynomials [28]. To represent the wavefunction in coordinate space, an equidistant grid in the range 3.0–25 au with 1024 gridpoints was used. In all simulations the desorbing part of the wavefunction is seperated by a grid-change technique. This method is based on an analytical propagation of the desorbing part of the wavefunction on a second grid in k space, where this part is analysed at a common final time

[29]. In this application of the gridchange the transfer function

$$f_{\text{trans}} = 1 - \frac{1}{1 + \exp\left[a(r - r_{\text{trans}}) \right]} \qquad (1)$$

with

$$a = 6.0 \text{ au}^{-1} \quad \text{and} \quad r_{\text{trans}} = 16.5 \text{ au}$$

was used. This transfer function is located at 16.5 au, which allows for a clear separation of adsorbed and desorbed parts of the wavepacket.

The initial vibrational eigenfunctions of the ground-state potential are calculated by a relaxation method based on an imaginary time propagation scheme [30].

As a first guess the one-dimensional model should be appropriate, but in a forthcoming paper the role of other coordinates (such as the polar angle between the molecular axis and the surface normal) will be discussed [31].

4.2. The potentials

As the wavepacket dynamics depend dramatically on the gradients and the relative position of the excited-state potential curve with respect to the ground state, a proper choice of the potential curves has to be made. For example, statements concerning the dependence of several experimentally observable quantities on the lifetime of representing wavepackets on the excited state (the resonance) are only valid if the knowledge on this state is on a sufficient theoretical basis. In the present study model potentials are constructed on the basis of ab-initio calculations of the NO/NiO(100) system.

The experimentally investigated system $NO/Cr_2O_3(0001)$ is similar to NO/NiO in a sense that the NO molecule is adsorbed in a non-linear adsorption geometry. Furthermore, we believe an NO^--like intermediate to be participating in the DIET process. For these reasons the potential energy curve of the excited state used in this work is derived from a charge transfer state that was calculated for the first time on a high-quality ab-initio basis for the system NO/NiO(100) [27]. A detailed investigation of the dynamics of nuclear motion and the construction of two-dimensional ab-initio potential energy surfaces for the NO/NiO(100) system from which the excited-state potential used in the present study can be derived will be published elsewhere [31].

The ground state consists of a simple Morse potential with a dissociation energy of $D_e = 0.036$ au. This value is consistent with the experimentally observed binding energy of nearly 1 eV. The equilibrium distance of $r_0 = 5.55$ au is a result of the ab-initio calculations of the system NO/NiO [31]. As Morse exponent $\alpha = 0.79$ au^{-1} was chosen in the following expression:

$$V_{\text{gr}}(r) = D_e\left[1 - \exp\{ -\alpha(r - r_0) \} \right]^2 - D_e . \qquad (2)$$

These potential energy curves are sketched in Fig. 2. In order to clarify the procedure presented in the next section, the coordinate-space expectation value of the vibrational ground state of the electronic ground state is shown as the Franck–Condon point on the excited-state curve.

4.3. Wavepacket propagations with fixed residence lifetimes

By wavepacket propagation in imaginary time [30] 17 vibrational eigenfunctions $\Psi_0(v)$ ($v = 0, \ldots, 16$) of the ground-state potential are calculated. These eigenfunctions are transferred separately onto the excited-state potential in a Franck–Condon-like manner, where the individual wavepackets are propagated under the influence of the excited-state Hamiltonian for a maximal time duration of one oscillation in the excited state. The wavepackets belonging to a fixed residence time t_r are separately transferred back onto the ground-state potential and propagated to a final common time of 2 ps. This procedure is repeated for each vibrational eigenstate of the electronic ground state.

In Fig. 3 the resulting desorption yield is shown as a function of fixed residence times in the excited state for the two vibrational states with $v = 0$ and $v = 1$. First of all, the different structure of the $v = 1$ curve, which is caused by the nodal structure of the $v = 1$ density, is noted. To illustrate this, the $v = 0$ and $v = 1$ densities, resulting after a propagation on

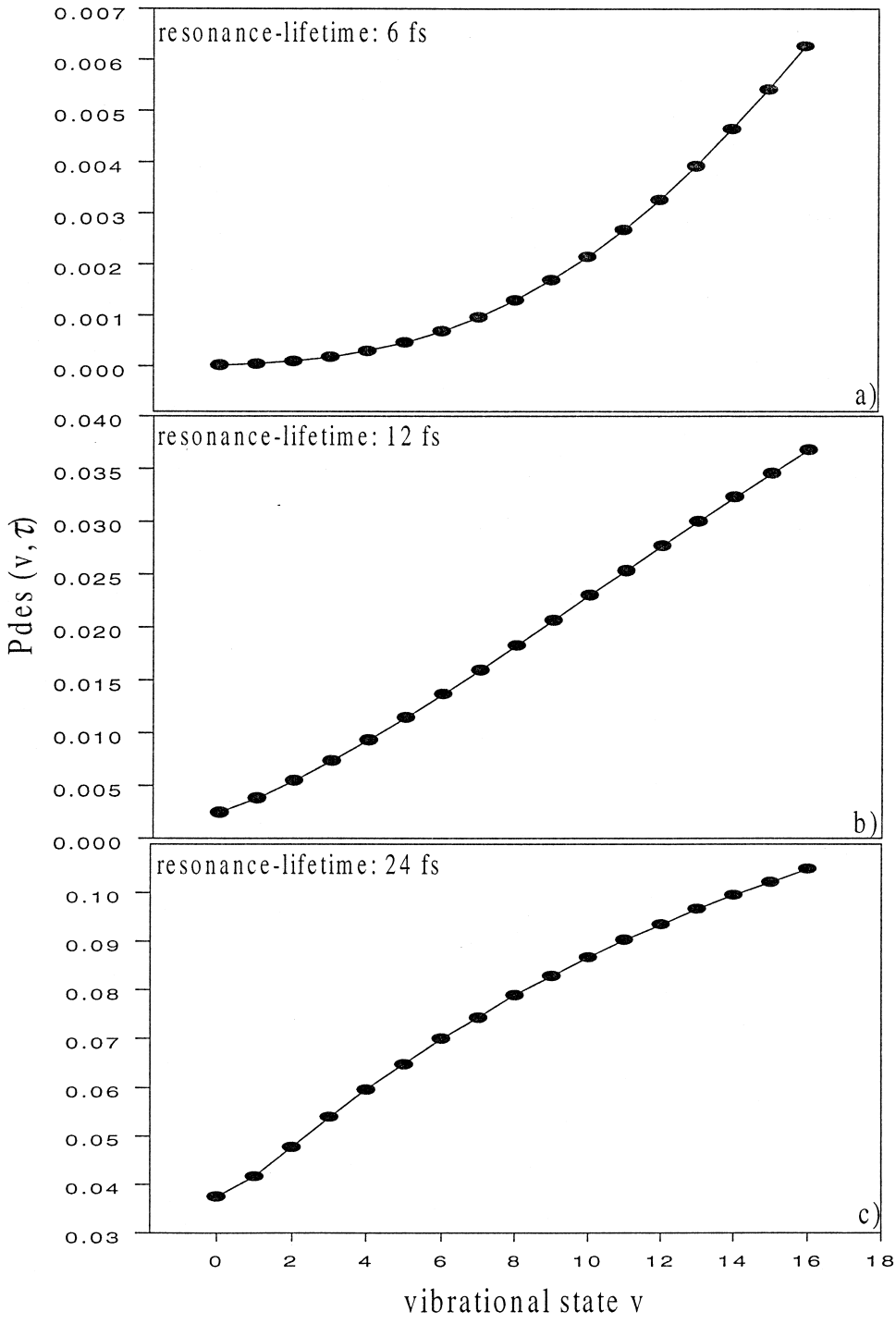

Fig. 7. Lifetime-weigted asymptotic desorption probability $P_{des}(v, \tau)$ for three *resonance lifetimes* τ as a function of the initial vibrational state v: (a) $\tau = 6$ fs; (b) $\tau = 12$ fs; and (c) $\tau = 24$ fs.

the excited state for 72 fs and a Franck–Condon backtransfer onto the ground-state potential curve, are shown in Fig. 4. The plateaus in the $v = 1$ curve (Fig. 3) are due to the fact that for the corresponding residence lifetimes the node of the $v = 1$ density is located in a region of the repulsive part of the ground-state potential where enough energy can be accumulated in order to allow for desorption.

Furthermore one realizes in Fig. 3 that in the case of residence times $t_r < 72$ fs (and $t_r > 120$ fs) the desorption probability is higher if the initial wavefunction is the $v = 1$ eigenfunction. In [10] it is analysed quantitatively for an Antoniewicz scenario that higher eigenstates of a one-dimensional ground-state potential can reach the repulsive region of the excited state within a shorter time than lower states do. The reason is the larger extension in coordinate space occupied by these higher eigenfunctions. Fig. 5a, where the desorption probability in case of the fixed residence lifetime of 48 fs is plotted as a function of the initial vibrational quantum number, confirms this analysis also for our potentials. Although fixed residence lifetimes are only unrealistic computational parameters, it is interesting to investigate the desorption probability for two more fixed residence lifetimes. In Fig. 5b and c the results for $t_r = 72$ fs and $t_r = 96$ fs are shown, respectively. The residence time of 96 fs corresponds to the turning point of the wavepacket in the excited state. While in case of short (and more realistic) residence lifetimes the larger extension in coordinate space of higher eigenstates increases the desorption yield (Fig. 5a), this larger extension in coordinate space becomes a disadvantage near the turning point. The lowest eigenstate, for example, is characterized by nearly 100% desorption, while the larger extension of higher eigenstates causes less desorption. Here the reason for this behaviour is that at the turning point, for example, only $\sim 50\%$ of the $v = 4$ wavefunction finds itself in a region of the repulsive part of the excited state, which allows for desorption after the Franck–Condon-like back transfer onto the ground state. To summarize, the large extension of vibrationally excited wavefunctions in the distance-coordinate increases desorption only during a certain period of time within the translation of the wavepacket in the excited state. The wavefunctions after the Franck–Condon backtransfer onto the ground-state potential are sketched in Fig. 6a and b for $t_r = 48$ fs and $t_r = 96$ fs, respectively.

If a lifetime of $t_r = 72$ fs is chosen, the two features discussed in this paragraph are important at the same time and a nearly flat curve results (Fig. 5b).

Finally, the higher the initial vibrational quantum number the less sensitive is the desorption yield to this quantum number. This is explained by arguing that in case of high excited states the square of the vibrational wavefunctions has its maxima at the classical turning points of the oscillation. Increasing the vibrational quantum number does not change the shape of the corresponding distribution significantly. Of course, only the very first few eigenstates are relevant in the thermal averaging procedure which allows comparison with experimental data.

It has to be mentioned again that a more reasonable and physical time parameter is an averaged lifetime of the excited state and this will be subject of the next section.

4.4. Averaged resonance lifetimes

In this section the lifetime-averaging procedure proposed by Gadzuk [32,33] will be applied. This is done by propagating 400 wavefunctions (only differing by their residence lifetime t_r in the excited state) for all 17 vibrational eigenstates on the electronic ground state, resulting in 6800 separate calculations. These wavefunctions correspond to a lifetime interval in the excited state between 0 and 193 fs (this is one complete oscillation of the initial wavepacket in the excited state). According to Gadzuk, any observ-

Fig. 8. Result of the summation (3) as a function of the maximum residence lifetime used in the lifetime averaging procedure: (a) $\tau = 6$ fs; (b) $\tau = 12$ fs; and (c) $\tau = 24$ fs. The inclusion of quantum trajectories with a residence lifetime t_r up to ~ 125 fs leads to a converged value for $P_{des}(\tau)$. To get rid of the dependence on the initial vibrational state, the result of (3) has been temperature-averaged already with the parameter $T = 300$ K. The residence lifetime $t_r = 72$ fs is indicated by the vertical line. At this residence lifetime the dependence of the unaveraged desorption probability on the initial vibrational state v changes roughly from an increasing to a decreasing behaviour.

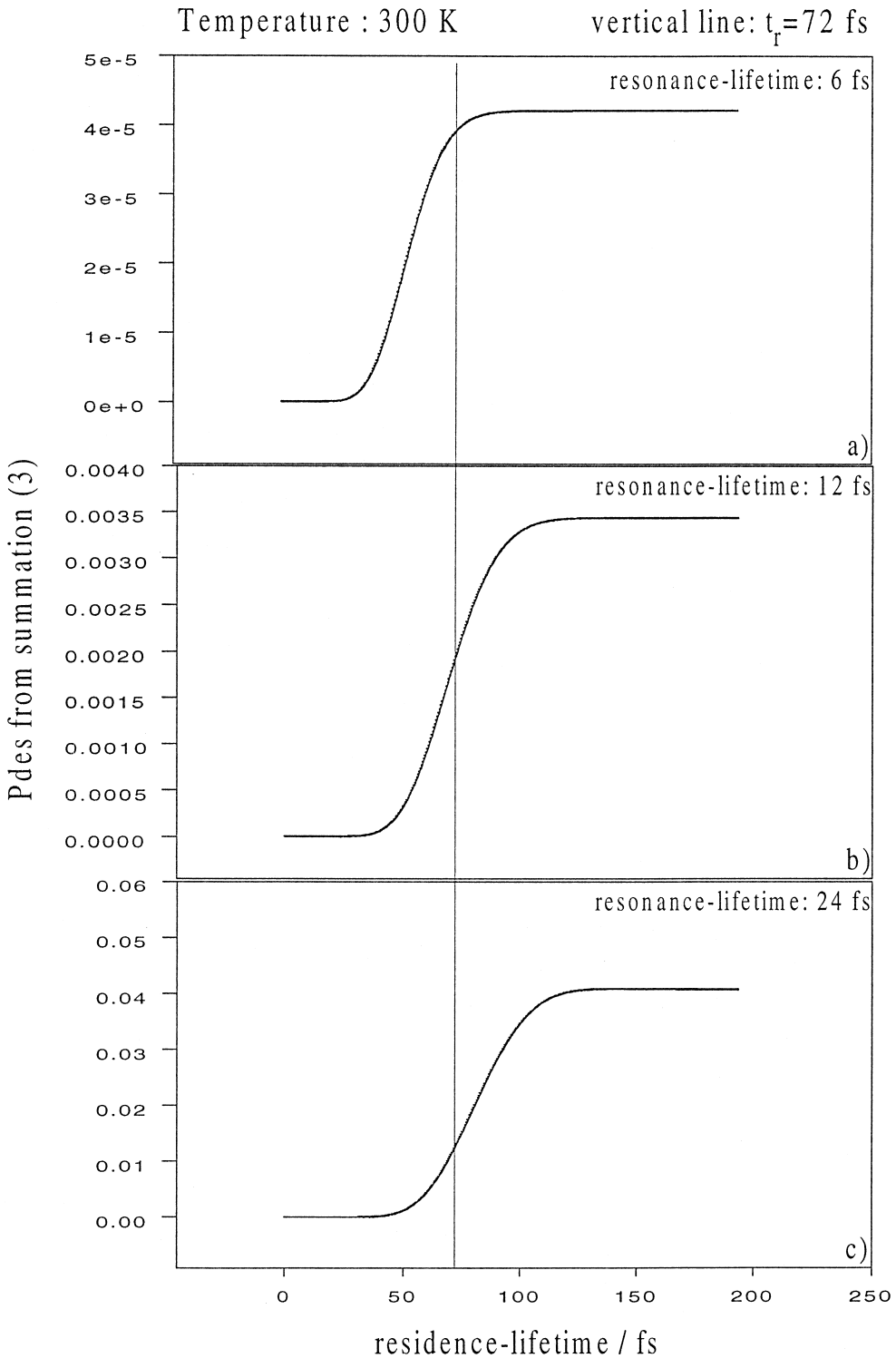
Temperature : 300 K
vertical line: t_r=72 fs
resonance-lifetime: 6 fs
resonance-lifetime: 12 fs
resonance-lifetime: 24 fs
a)
b)
c)
Pdes from summation (3)
residence-lifetime / fs
5e-5
4e-5
3e-5
2e-5
1e-5
0e+0
0.0040
0.0035
0.0030
0.0025
0.0020
0.0015
0.0010
0.0005
0.0000
0.06
0.05
0.04
0.03
0.02
0.01
0.00
0
50
100
150
200
250

able A is averaged with respect to the resonance lifetime τ by guessing an exponential decay of the excited-state population:

$$A(\tau) = \frac{\sum_{n=1}^{N} A(t_n) \exp(-t_n/\tau)}{\sum_{n=1}^{N} \exp(-t_n\tau)} . \quad (3)$$

The index n accounts for the quantum trajectory with the fixed residence lifetime t_n. As mentioned before, N equals 400 in this averaging procedure.

In Fig. 7a, b and c the averaged desorption yields for the exemplary resonance lifetimes $\tau = 6$, 12 and 24 fs, respectively, are presented as a function of the initial vibrational state. In all cases the averaged desorption yield increases with the vibrational quantum number v. This is reasonable, because specially in case of the resonance lifetimes 6 and 12 fs those quantum trajectories which belong to residence lifetimes shorter than 72 fs can be shown to be mainly relevant in the lifetime-averaging procedure. To demonstrate this, Fig. 8 shows the results of the summation (3) as a function of the residence lifetime t_r for all three resonance lifetimes. The temperature averaging procedure ($T = 300$ K) that will be presented in the next section has been performed in this case already in order to include all vibrational eigenstates at the same instance. First of all it is clearly seen that a maximum residence lifetime of 190 fs yields a converged result in all cases. Then the role of residence lifetimes with $t_r > 72$ fs has to be emphazised. In the last paragraph it has been shown that roughly at this residence lifetime *the desorption yield as a function of the initial vibrational eigenstate changes from an inreasing behaviour to a more or less decreasing behaviour* (Fig. 5a–c). This 'critical residence lifetime' $t_r = 72$ fs is indicated in Fig. 8 with a vertical line. It must be recognized that residence lifetimes, which decrease the desorption yield as a function of the initial vibrational state (namely those with $t_r > 72$ fs) begin to play a more and more important role in the averaging procedure in case of relative large resonance lifetimes as for example 24 fs. This resonance lifetime is not too unrealistic, because it yields desorption probabilities on the experimental order of magnitude. To summarize, the increase in the desorption yield as a function of the vibrational quantum number (Fig. 7) is influenced by the choice of the resonance lifetime in Gadzuk's averaging procedure. As a measure of this increase $P_{des}(\nu = 16)/P_{des}(\nu = 0)$ is calculated and yields the values 525, 15 and 3 if the resonance lifetimes are 6, 12 and 24 fs, respectively. In case of $\tau = 24$ fs the relative small factor can be explained in terms of the weight of those residence lifetimes, which account for an decrease in the desorption yield as a function of the initial vibrational state (see Fig. 5c).

This section dealt with lifetime weighted desorption probabilities as a function of the initial vibrational state. In order to allow comparison with experimental data, the influence of temperature on the last results has to be investigated in the next section.

4.5. Boltzmann weighting

The lifetime-averaged results of the last section will be connected with the influence of the temperature T by guessing a Boltzmann distribution of the initial vibrational eigenstates. This leads to an averaging procedure for the observable $A(\tau)$, where the weighting function is the Boltzmann factor $\exp(-E_v/kT)$:

$$\bar{A}(\tau, T) = \frac{\sum_{v=0}^{N} A(\tau) \exp(E_v/kT)}{\sum_{v=0}^{N} \exp(-E_v/kT)} . \quad (4)$$

The propagation of 17 vibrational eigenfunctions

Table 1
Relative population P_v/P_0 of the initial ground-state vibrational level v for $T = 350$ K and $T = 100$ K

	$T = 350$ K	$T = 100$ K
$v = 0$	1.0000	1.0000
$v = 1$	0.4455	0.0590
$v = 2$	0.2005	0.0036
$v = 3$	0.0973	0.0002
$v = 4$	0.0419	2×10^{-5}
$v = 5$	0.0194	1×10^{-6}
$v = 6$	0.0091	7×10^{-8}
$v = 7$	0.0043	5×10^{-9}
$v = 8$	0.0021	4×10^{-10}
$v = 9$	0.0010	3×10^{-11}
$v = 10$	0.0005	3×10^{-12}
$v = 11$	0.0002	2×10^{-13}
$v = 12$	0.0001	2×10^{-14}

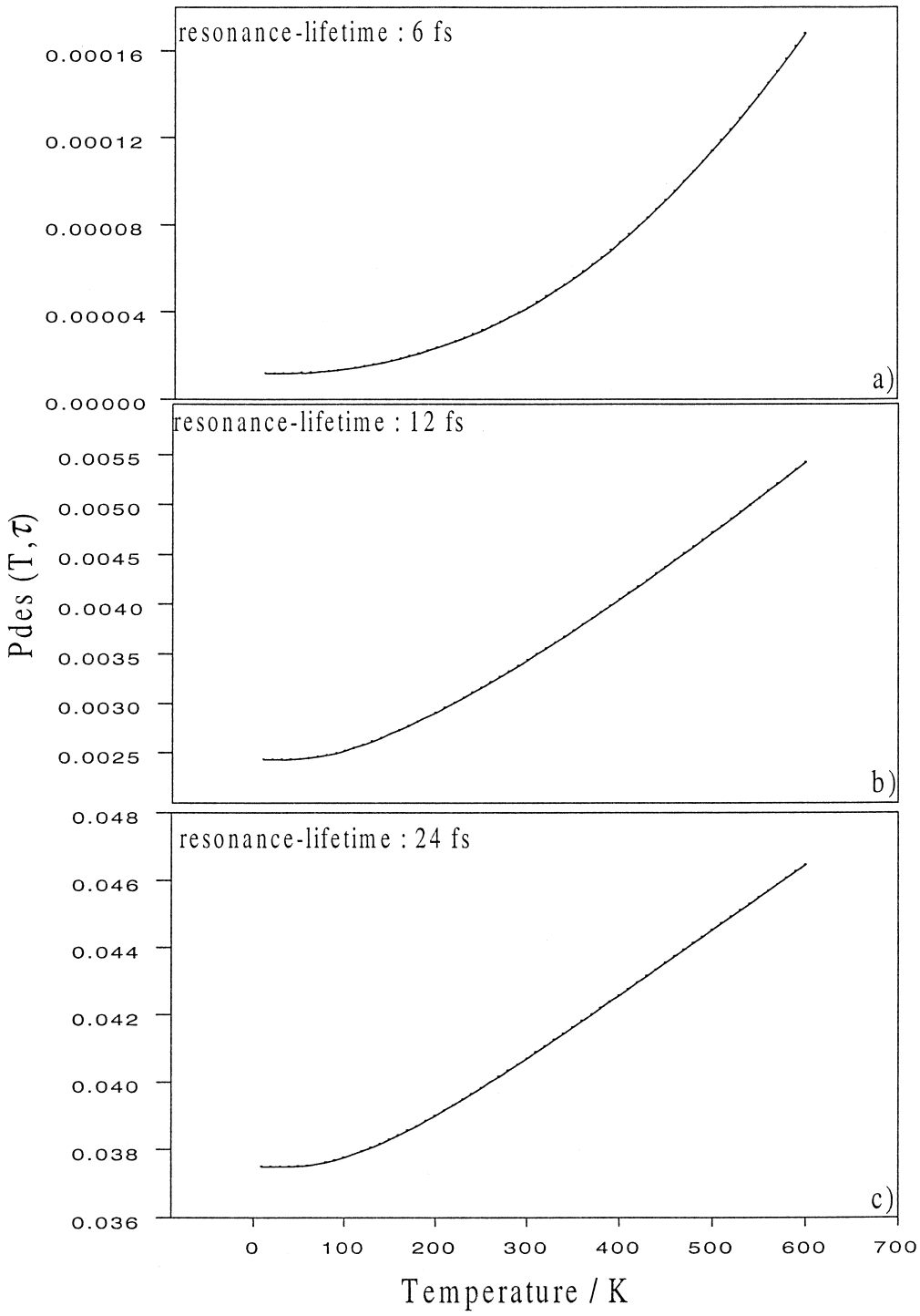

Fig. 9. Temperature-averaged desorption probability $P_{des}(T, \tau)$ for three *resonance lifetimes* τ as a function of temperature T: (a) $\tau = 6$ fs; (b) $\tau = 12$ fs; and (c) $\tau = 24$ fs.

was sufficient to investigate a temperature interval between 0 and 600 K. For the relative populations of the vibrational energy levels see Table 1, where these values are collected for the two temperatures $T = 100$ K and $T = 350$ K, the desorption temperature found in thermal desorption spectra being in the range 340 ± 20 K. The temperature dependence of the averaged desorption yield is illustrated in Fig. 9. Again the sample resonance lifetimes 6, 12 and 24 fs were chosen. In all cases a clear increase in the desorption yield after the incorporation of the temperature parameter is obvious.

The experimental cross-section, which is on the order of 1×10^{-17} cm^2 (1–4 orders of magnitude larger than in the case of metals) is consistent with a desorption yield per excitation event on the order of 0.01. This fact is the basis to estimate a resonance lifetime in the range between 12 and 24 fs. This range, which seems to be reasonable in case of this oxide system [27] is located at higher values than the lifetimes that are estimated in some cases for metallic systems in one-dimensional treatments.

Nevertheless, the most dramatic effect of increasing temperature on the desorption probability is seen in Fig. 9a. An increase in temperature from 100 to 300 K yields an increase in the desorption probability by a factor 3, if a resonance lifetime of 6 fs is chosen. This factor is reduced to 1.4 and 1.1 for resonance lifetimes of 12 and 24 fs, respectively. This behaviour can be directly traced back to the different dependences of the desorption yields on the fixed vibrational quantum numbers that was discussed in the last section and was illustrated in the Fig. 5a–c. The different factors of the last paragraph are still 'visible' after a temperatur-averaging procedure. In the case of short resonance lifetimes (6 fs) only the quantum trajectories which increase the desorption probability as a function of the initial

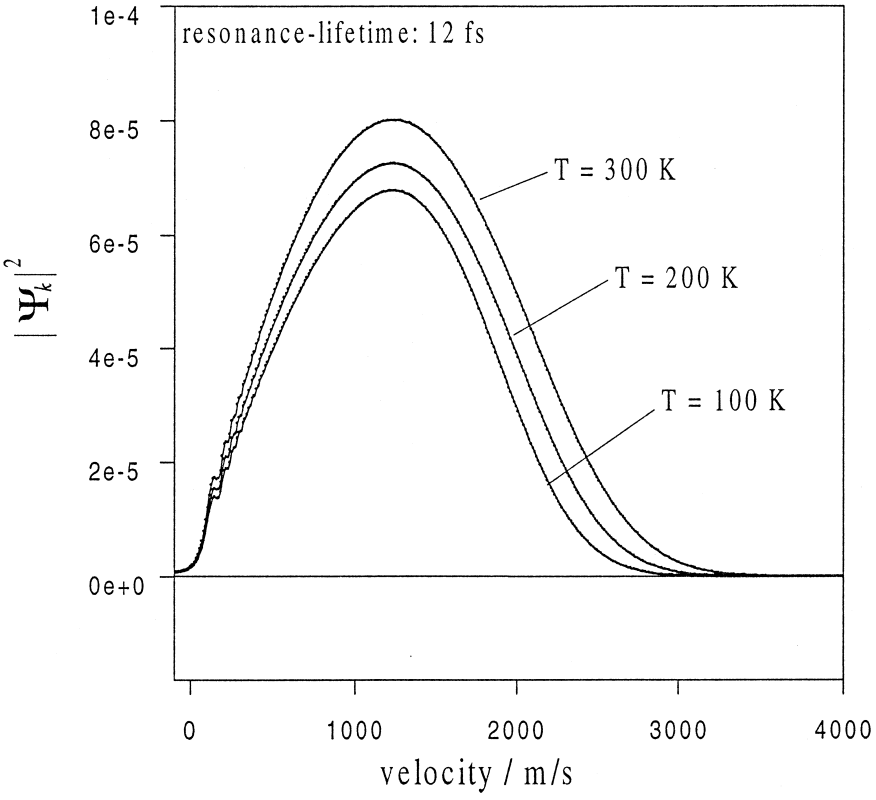

Fig. 10. Temperature dependence of the lifetime-averaged velocity distributions in the case of $\tau = 12$ fs. Shown are velocity distributions for $T = 100$, 200 and 300 K.

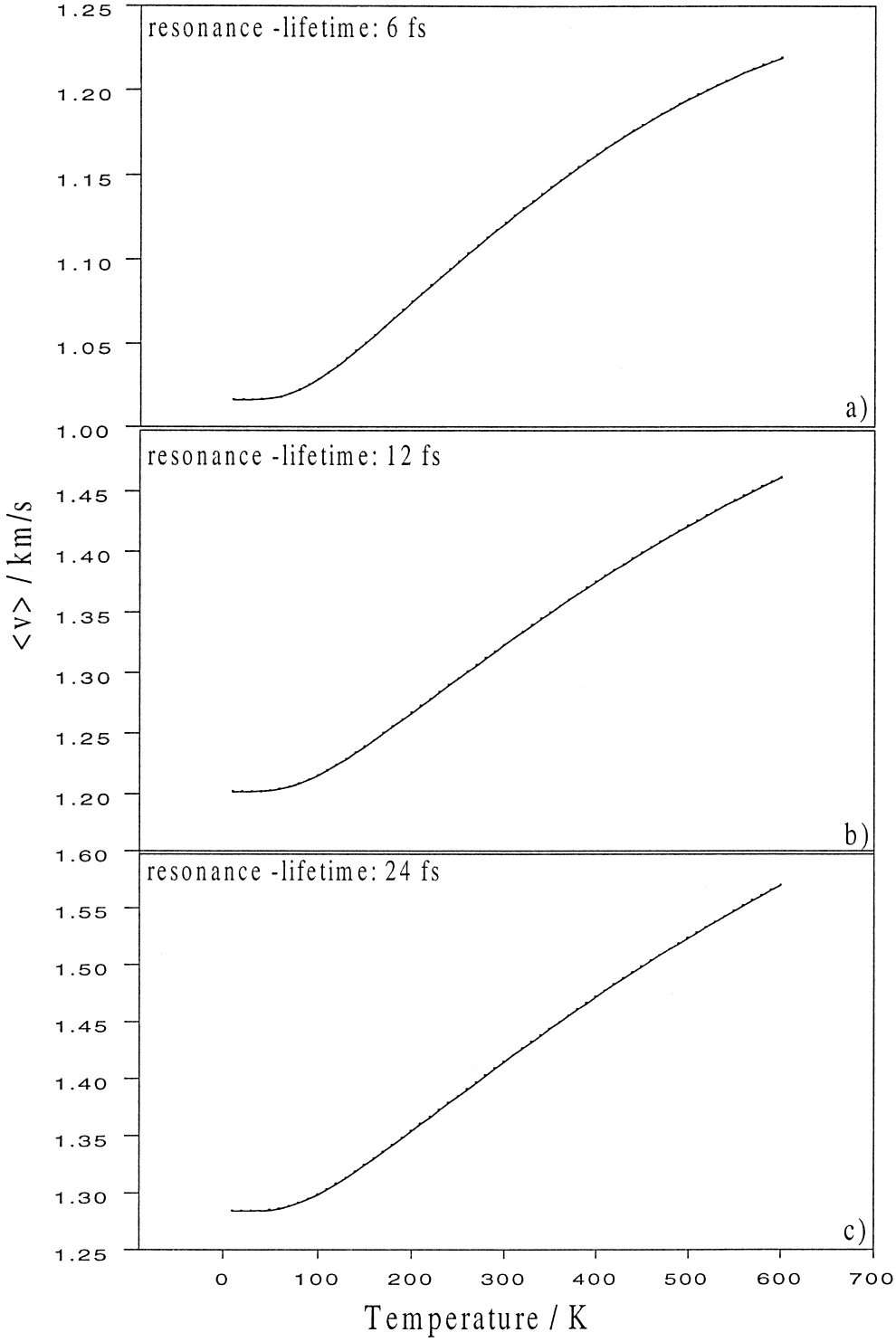

Fig. 11. Temperature dependence of the mean velocities $\langle v \rangle$, deduced from the calculated velocity distributions, for three *resonance lifetimes* τ: (a) $\tau = 6$ fs; (b) $\tau = 12$ fs; and (c) $\tau = 24$ fs.

vibrational state are relevant. If the resonance lifetime is increased, the influence of quantum trajectories with the opposite behaviour grows.

Summarizing, a reasonable choice of the resonance lifetime is 12 fs. Larger values lead to a better agreement with the absolute experimental cross-section, but reduce the temperature effects, which we mainly focus upon in this paper.

Another experimentally observable quantity is the velocity distribution of the desorbing species. From these distributions mean values of the velocity can easily be derived. For this reason, the lifetime-averaging procedure, followed by thermal weighting was applied to the momentum-space density of the desorbed part of the wavefunctions, which have reached the asymptotic region of the ground-state potential. After the analytical propagation to a common final time on the second grid these resulting momentum-space densities can be interpreted as velocity distributions of the desorbing NO molecules. As these distributions are an observable quantity, it is reasonable to proceed in the same manner as with the desorption probability [34].

In Fig. 10 the influence of temperature on the velocity distributions is demonstrated. The distributions resulting in case of the resonance lifetime 12 fs are shown for the temperatures 100, 200 and 300 K. At a first glance only the increase in the desorption probability as a function of the temperature is confirmed, because this quantity scales with the area enclosed by the velocity distribution. A more detailed analysis reveals a slight dependence of the mean velocity on the temperature. Fig. 11 shows expectation values of the lifetime- and temperature-averaged velocity distributions as a function of the temperature again for the three exemplary resonance lifetimes 6, 12 and 24 fs. In all cases the mean velocity increases if temperature is enhanced. The absolute increase is in the same order of magnitude as the experimentally observed behaviour. Although this result is encouraging, it should be realized that the absolute value of the mean velocities is too high. Reasons for this might be the one-dimensional treatment or the lack of any precursor states in our simulations. We believe that those states should be discussed in terms of a multidimensional model in order to explain the shape of the experimentally observed velocity distributions. Precursor states could play the role of an energy trap accounting for the peaking of the velocity distributions at relative small velocities. A detailed theoretical investigation of the role of precursor states in laser-induced desorption will be published elsewhere [35].

5. Conclusions

Performing time-dependent wavepacket studies we have shown that the experimentally observed dependence of quantities like desorption cross-section or mean velocities of the desorbing species on temperature can be explained in terms of a pure quantum mechanical picture. The trend of an increase in desorption yield and velocity as a function of temperature is visible even after carrying out two averaging procedures, which tend to allow for a realistic comparison with experiment. The two parameters in the averaging procedures were the resonance lifetime τ of the excited state and the temperature T. It is shown in case of our system that short resonance lifetimes have more pronounced relative effects on the dependence of the observables on temperature than longer, not too unrealistic resonance lifetimes. The temperature effects on the desorption probability become less pronounced if residence lifetimes of the representing wavepacket in the excited state with a negative influence on the desorption probability become relevant. In our $NO/Cr_2O_3(0001)$ system all these effects have to be discussed, because only quite large resonance lifetimes are consistent with the observed desorption cross-sections. The microscopic reason is the weak gradient of the ab-initio excited-state potential used in the presented simulations. A resonance lifetime of $\tau = 12$ fs accounts for an increase in the desorption probability by a factor of 1.4 and yields absolute values of P_{des} which are slightly too small. One has to consider on the other hand that the exact correlation between the measured desorption cross-section and the calculated desorption probability per resonance event is not known.

Due to the fact that in the presented simulations the temperature effects become more pronounced if the resonance lifetime of the excited state is shortened, one would guess that another temperature dependence is observed for example in the case of metals, where the resonance lifetimes are believed to be smaller than 10 fs.

Acknowledgements

We would like to thank R. Kosloff and V. Staemmler for many helpful and stimulating discussions. The work was financially supported by the Deutsche Forschungsgemeinschaft through the Graduiertenkolleg 'Dynamische Prozesse an Festkörperoberflächen' and by the German–Israeli Foundation (GIF).

References

[1] T.J. Chuang, H. Seki, I. Hussla, Surf. Sci. 158 (1985) 525.
[2] V.S. Letokhov, Science 180 (1973) 451.
[3] R.L. Van der Wal, J.L. Scott, F.F. Crim, J. Chem. Phys. 92 (1990) 803.
[4] R.N. Zare, J.H. Hahn, R. Zenobi, Bull. Chem. Soc. Jpn. 61 (1988) 87.
[5] F.M. Zimmermann, W. Ho, Surf. Sci. Rep. 22 (1995) 127.
[6] K. Al-Shamery, H.-J. Freund, Curr. Opin. Solid State Mater. Sci. 1/5 (1996) 622.
[7] K. Al-Shamery, Appl. Phys. A, Mater. Sci. Proc. 63 (1996) 509.
[8] Q.-S. Xin, X.-Y. Zhu, Chem. Phys. Lett. 265 (1997) 259.
[9] J. Manz, P. Saalfrank, B. Schmidt, J. Chem. Soc., Faraday Trans. 93 (1997) 957.
[10] C. Daniel, R. de Vivie-Riedle, M.-C. Heitz, J. Manz, P. Saalfrank, Int. J. Quant. Chem. 57 (1996) 595.
[11] J.P. Culver, M. Li, Z.-J. Sun, R.M. Hochstrasser, A.G. Yodh, Chem. Phys. 205 (1996) 159.
[12] T.A. Germer, J.C. Stephenson, E.J. Heilweil, R.R. Cavanagh, J. Chem. Phys. 98 (1993) 9986.
[13] T.A. Germer, J.C. Stephenson, E.J. Heilweil, R.R. Cavanagh, J. Chem. Phys. 101 (1994) 1704.
[14] R.R. Cavanagh, D.S. King, J.C. Stephenson, T.F. Heinz, J. Phys. Chem. 97 (1993) 786.
[15] F.-J. Kao, D.G. Busch, D. Gomes da Costa, W. Ho, Phys. Rev. Lett. 70 (1993) 4098.
[16] S. Deliwala, R.J. Finlay, J.R. Goldman, T.H. Her, W.D. Mieher, E. Mazur, Chem. Phys. Lett. 242 (1995) 617.
[17] M. Menges, B. Baumeister, K. Al-Shamery, H.-J. Freund, C. Fischer, P. Andresen, Surf. Sci. 316 (1994) 103.
[18] M. Wilde, K. Al-Shamery, H.-J. Freund (paper in preparation).
[19] D.C. Jacobs, R.N. Zare, J. Chem. Phys. 85 (1986) 5457.
[20] M. Wilde, O. Seiferth, K. Al-Shamery, H.-J. Freund (paper in preparation).
[21] C. Xu, M. Hassel, H. Kuhlenbeck, H.-J. Freund, Surf. Sci. 258 (1991) 23.
[22] P. Saalfrank, S. Holloway, G.R. Darling, J. Chem. Phys. 103 (1995) 6720.
[23] P. Saalfrank, T. Klamroth, Ber. Bunsenges., Phys. Chem. 99 (1995) 1347.
[24] P. Saalfrank, Chem. Phys. 193 (1995) 119.
[25] P. Saalfrank, R. Baer, R. Kosloff, Chem. Phys. Lett. 230 (1994) 463.
[26] P. Saalfrank, R. Kosloff, J. Chem. Phys. 105 (1996) 2441.
[27] T. Klüner, H.-J. Freund, J. Freitag, V. Staemmler, J. Chem. Phys. 104 (1996) 10030.
[28] H. Tal-Ezer, R. Kosloff, J. Chem. Phys. 81 (1984) 3967.
[29] R. Heather, H. Metiu, J. Chem. Phys. 86 (1987) 363.
[30] R. Kosloff, H. Tal-Ezer, Chem. Phys. Lett. 127 (1986) 223.
[31] T. Klüner et al. (unpublished).
[32] J.W. Gadzuk, L.R. Richter, S.A. Buntin, D.S. King, R.R. Cavanagh, Surf. Sci. 235 (1990) 317.
[33] J.W. Gadzuk, Surf. Sci. 342 (1995) 345.
[34] R. Kosloff (private communication).
[35] T. Klüner et al. (unpublished).